Supporting information belonging to the paper:

Rh-Mediated Carbene Polymerization: From Multistep Catalyst Activation to Alcohol-Mediated Chain-Transfer

Annemarie J. C. Walters,[a] Erica Jellema,[a] Markus Finger,[a,b] Petra Aarnoutse,[a] Jan M. M. Smits,[c] Joost N. H. Reek[a] and Bas de Bruin[,a]*

[a] Van 't Hoff Institute for Molecular Sciences (HIMS), University of Amsterdam, PO Box 94720 1090 GE Amsterdam, [b] Dutch Polymer Institute DPI, PO Box 902 5600 AX, Eindhoven and [c] Institute for Molecules and Materials, Radboud University Nijmegen, Heyendaalseweg 135, 6525 AJ Nijmegen, the Netherlands

S1. Additional characterization of [Rh(cod)(Mes)(PPh_3)] and [Rh(hxd)(L-pro)] 2

1-A. [Rh(cod)(Mes)(PPh_3)] (8) *2*

1-B. [Rh(hxd)(L-pro)] (4) *2*

S2. Additional characterization of the oligomer fraction 4

2-A. IR spectroscopy *4*

2-B. Elemental Analysis *5*

S3. MALDI-TOF mass spectrometry 6

3-A. Assigned series *6*

3-B. MALDI-ToF mass spectra *8*

S4. SEC traces 25

S5. Characterization of the MeOH soluble material obtained in the presence of alcohols 27

S1. Additional characterization of [Rh(cod)(Mes)(PPh_3)] and [Rh(hxd)(L-pro)]

1-A. [Rh(cod)(Mes)(PPh_3)] (8)

Crystals of [Rh(cod)(Mes)(PPh_3)] suitable for X-ray diffraction were obtained by crystallization from *n*-hexane. The molecular structure and selected bond distances and angles are depicted in Figure S1-1 and Table S1-1. [Rh(cod)(Mes)(PPh_3)] exhibits a square planar environment around rhodium and has bond lengths and angles similar to related complexes in the literature.[1,2]

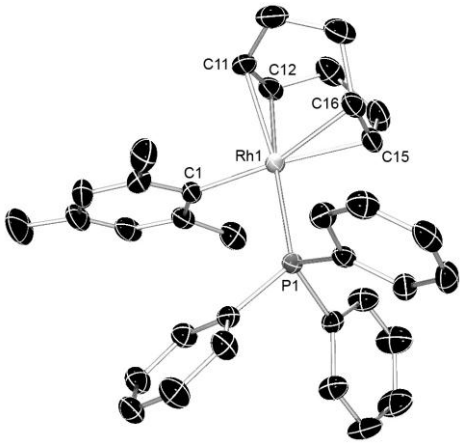

Figure S1-1. Molecular structure of [Rh(cod)(Mes)(PPh_3)] (**8**) with 50% probability ellipsoids. Hydrogen atoms are omitted for clarity.

Table S1-1. Selected bond lengths (Å) and angles (º) of [Rh(cod)(Mes)(PPh_3)].

Rh(1)–P(1)	2.3153(9)
Rh(1)–C(1)	2.056 (3)
Rh(1)–C(11)	2.194(3)
Rh(1)–C(12)	2.201(3)
Rh(1)–C(15)	2.202(3)
Rh(1)–C(16)	2.253(3)
C(11)–C(12)	1.361(5)
C(15)–C(16)	1.365(5)
C(1)–Rh(1)–P(1)	90.83(8)
C(1)–Rh(1)–C(11)	86.90(13)
P(1)–Rh(1)–C(11)	160.51(10)

1-B. [Rh(hxd)(L-pro)] (4)

B1. NMR:

[Rh(hxd)(L-pro)] is present in two different isomers in solution. The ^{1}H and ^{13}C NMR spectra show them in a 1:1 ratio (Figure S1-2). These isomers can interconvert by rotation of the hexadiene ligand.

[1] Yamamoto, M.; Onitsuka, K.; Takahashi, S. *Organometallics* **2000**, *19*, 4669.

[2] Lahoz, F. J.; Martin, E.; Tiburcio, J.; Torrens, H.; Terreros, P. *Transition Met. Chem.* **1994**, *19*, 381.

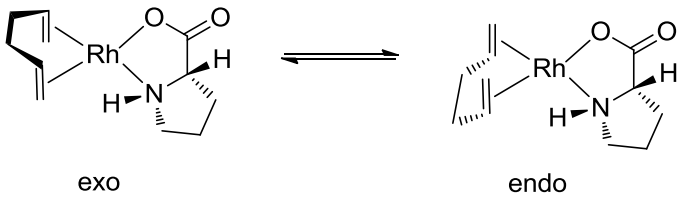

exo endo

Figure S1-2. Two isomers of **4** observed in solution.

B2. X-Ray structure

[Rh(hxd)(L-pro)] was analyzed by X-ray diffraction and the molecular structure is shown in Figure S1-3 with selected bond distances and angles in Table S1-2. In the crystal only the *exo* isomer is observed. Similarly to related structures it adopts a square planar geometry.[3,4] Furthermore, the structure is isostructural to its cyclooctadiene analogue and it shows a slightly bent prolinate ring.

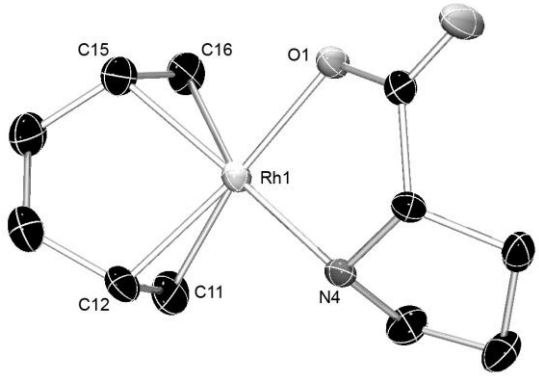

Figure S1-3. Molecular structure of [Rh(hxd)(L-pro)] (**4**) with 50% probability ellipsoids. Hydrogen atoms are omitted for clarity.

Table S1-2**.** Selected bond lengths (Å) and angles (°) of [Rh(hxd)(L-pro)] (**4**).

Rh(1)–N(4)	2.092(2)
Rh(1)–O(1)	2.060(2)
Rh(1)–C(11)	2.102(4)
Rh(1)–C(12)	2.110(3)
Rh(1)–C(15)	2.159(3)
Rh(1)–C(16)	2.128(3)
C(11)–C(12)	1.385(5)
C(15)–C(16)	1.374(4)
N(4)–Rh(1)–O(2)	81.14(8)
O(1)–Rh(1)–C(11)	164.88(12)
N(4)-Rh(1)-C(11)	95.59(10)

[3] Hetterscheid, D. G. H.; Hendriksen, C.; Dzik, W. I.; Smits, J. M. M.; van Eck, E. R. H.; Rowan, A. E.; Busico, V.; Vacatello, M.; Van Axel Castelli, V.; Segre, A.; Jellema, E.; Bloemberg, T. G.; de Bruin, B. *J. Am. Chem. Soc.* **2006**, *128*, 9746.

[4] Leipoldt, J. G.; Grobler, E. C. *Inorg. Chim. Acta* **1983**, *72*, 17.

S2. Additional characterization of the oligomer fraction

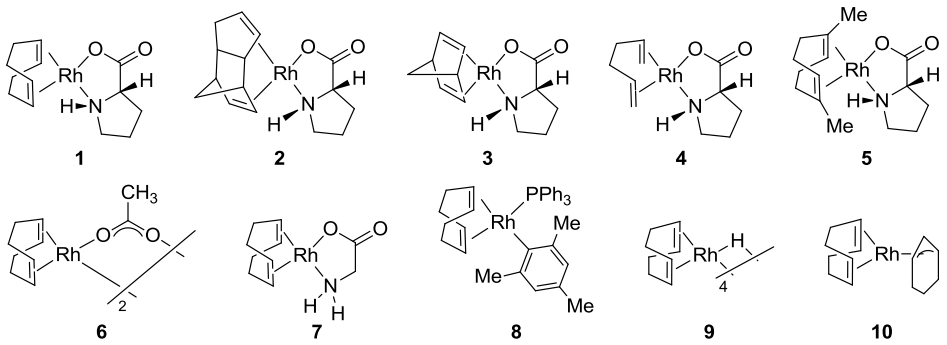

Figure S2-1. Selection of the catalyst precursors used for the polymerization of EDA

2-A. IR spectroscopy[5]

The IR spectra of the polymer and the oligomers are similar (Figure S2-2), with the most significant differences being additional vibrations for the oligomeric species at ~1600 cm^{-1} and ~1200 cm^{-1}. In this sample, no dimers were present, as was evidenced by NMR spectroscopy. We cannot exclude that these signals stem from the proline ligand or its derivatives. However, in view of the high Rh content (see below), these extra signals might well be indicative of oligomer ester moieties coordinated to Rh.

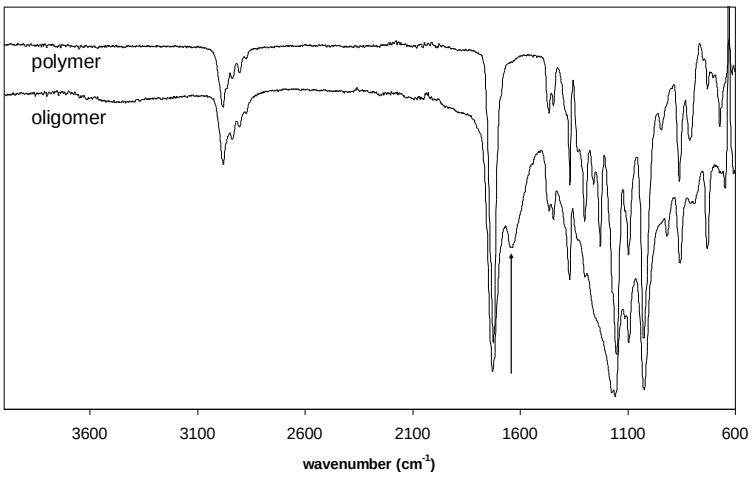

Figure S2-2. IR spectrum of polymeric and oligomeric products of a reaction of **1** with EDA.

[5] IR solid state spectroscopy measurements were performed on a Shimadzu FTIR 8400S spectrometer equipped with a Specac MKII Golden Gate Single Reflection ATR system.

2-B. Elemental Analysis[6]

The Rh content of the polymer and oligomer fractions was analyzed by elemental analysis (Table S2-1). The analysis of the polymer confirms the calculated composition and shows only negligible amounts of Rh (entry 2).[3] On the other hand, rhodium is clearly present in the methanol soluble fraction of the reaction mixture of **1**. The rhodium:oligomer ratio in entry 4 corresponds roughly to the one expected if all of the catalyst remains in the oligomer fraction including proline and cyclooctadiene (or their derivatives). After filtration over silica, the Rh content is still very high (entry 5) suggesting that a large part of the Rh species is strongly bound to the oligomers. These high numbers (~0.5-1 Rh atoms per oligomeric chain) leave the possibility of rhodium still being covalently attached to the oligomeric chains as one of the chain ends.

Table S2-1. Elemental analyses of polymer and oligomers of EDA.

entry	polymer/oligomer	precatalyst		C	H	N	Rh
1	Polymer		calculated	55.81	7.02	-	-
2	Polymer	**1**	found	55.67	6.91	n.d.	0.09
3	Oligomer	**2**	found	51.11	6.24	1.47	n.d.
4	Oligomer	**1**	found	51.22	6.36	1.19	5.46
5[a]	Oligomer	**1**	found	49.77	6.26	0.81	4.50

[a] Filtrated over silica before analysis.

[6] Elemental analyses (CHN) were performed by the Kolbe analytical laboratory in Mülheim an der Ruhr (Germany).

S3. MALDI-TOF mass spectrometry

3-A. Assigned series

The MALDI-ToF mass spectra were analyzed for the following series:

A: saturated chain with hydrogen end-groups: [H—$(CHCO_2Et)_n$—H]

A1 – Li^+ as charge carrier

A2 – Na^+ as charge carrier

A3 – K^+ as charge carrier

A4 – Rh^+ as charge carrier

A5 – $Rh(olefin)^+$ as charge carrier (olefin = cod, dcp, dmcod, hxd, nbd)

B: saturated chain with an EtO end-group: [H—$(CHCO_2Et)_n$—OEt]

B1 – Li^+ as charge carrier

B2 – Na^+ as charge carrier

B3 – K^+ as charge carrier

B4 – Rh^+ as charge carrier

C: saturated chain with a HO end-group: [H—$(CHCO_2Et)_n$—OH]

C1 – Li^+ as charge carrier

C2 – Na^+ as charge carrier

C3 – K^+ as charge carrier

C4 – Rh^+ as charge carrier

D: unsaturated chain with a hydrogen and a vinylic end-group: [H—$(CHCO_2Et)_n$—$C(CO_2Et)=CHCO_2Et$]

D1 – Li^+ as charge carrier

D2 – Na^+ as charge carrier

D3 – K^+ as charge carrier

D4 – Rh^+ as charge carrier

D5 – $Rh(olefin)^+$ as charge carrier (olefin = cod, dcp, dmcod, hxd, nbd)

D6 – H^+ as charge carrier

E: saturated chain with the anionic ligand of the catalyst as end-group:

[H—$(CHCO_2Et)_n$—Y] (*i.e.* Y = AcO for **15** and Y = Mes for **7**)

E1 – Li^+ as charge carrier

E2 – Na^+ as charge carrier

E3 – K^+ as charge carrier

E4 – Rh^+ as charge carrier

These series were chosen according to the series that we could find before. The following points had to be considered in the interpretation of the spectra:

All elements have similar isotopic patterns, so that in case of equal mass it is hard to differentiate between them. However, by addition of CF_3CO_2Li and CF_3CO_2Na the proposed series can be established clearly. There are the following remaining ambiguities:

- The mass difference between Li – Na and Na – K is 16, which means that C1, A2 and C2, A3 have equal masses. After addition of Li or Na salts it appears most likely that the corresponding ions are present, while Li^+ series are absent otherwise. We assigned the signals accordingly (see Figure S3-2, Figure S3-3, Figure S3-5, Figure S3-9, Figure S3-11 and Figure S3-14).
- The mass of D3 (an unsaturated chain with K^+ as charge carrier) corresponds to an unsaturated chain with $Rh(cod)^+$ (D5), an unsaturated chain with a HO end-group and Na^+ as charge carrier or a saturated chain with a MeO end-group and Li^+ as charge carrier (created in the work-up). Li^+ appears unlikely when it is not added and this series indeed does not occur after addition of Li salt. The same is true for an unsaturated chain with a HO end-group, because the D3 series disappears after addition of Na^+ (see Figure S3-3 and Figure S3-14). Additionally, this series is observed regardless if the experiment was conducted under inert conditions with carefully dried solvents and substrate or just in air. On the other hand, D3 does not occur in any case when the cod ligand was not present in the catalyst. We therefore believe that this series is actually D5(cod). This can be confirmed in case of **2**, **4** and **5**, where D5 is detected as well but less distinctive, this time with the corresponding diene (see Figure S3-1, Figure S3-6, Figure S3-7 and Figure S3-12). The ligand should be easily lost and indeed D4 is nearly always present besides D5 (see Figure S3-1, Figure S3-6, Figure S3-7, Figure S3-12, Figure S3-15 and Figure S3-17).
- The mass of D4 corresponds to either $[H—(CHCO_2Et)_n—CO_2Et=CHCO_2Et]$ with Rh^+ as charge carrier or $[HO—(CHCO_2Et)_n—CO_2Et=CHCO_2Et]$ with H^+ as charge carrier. Here, the same argumentation holds as for D3, for which reason we believe that Rh^+ is the charge carrier in this series.
- We did consider K^+ as charge carrier, however we believe now that it does play only a minor role because there is no unambiguous series. We decided accordingly against K^+.
- For **3**, $Rh(nbd)^+$ and Na^+ would give the same series when present as charge carrier.

3-B. MALDI-ToF mass spectra

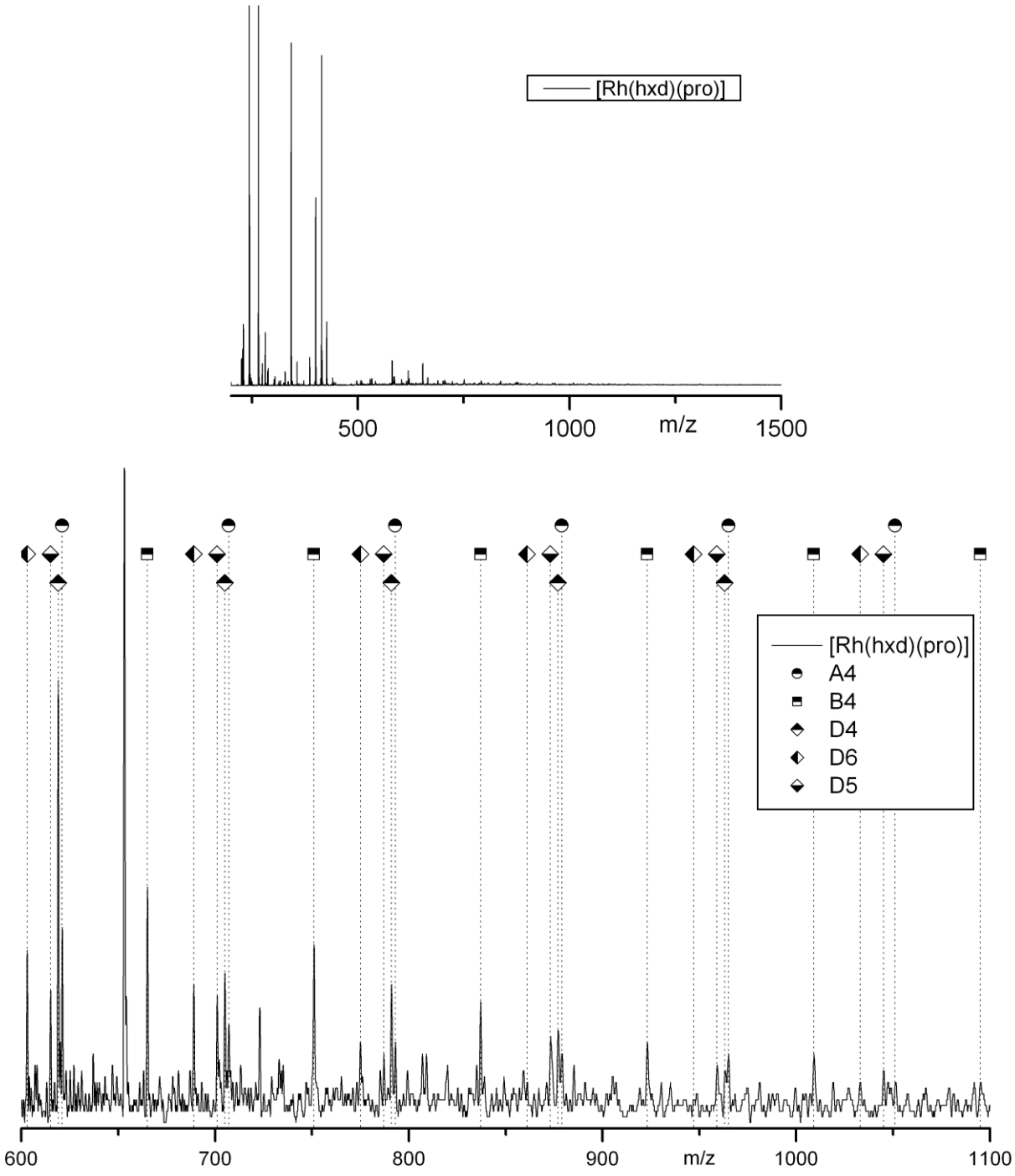

Figure S3-1: MALDI-ToF mass spectra of [Rh(hxd)(L-pro)] (**4**), complete spectrum (above) and selected part with assigned series (below).

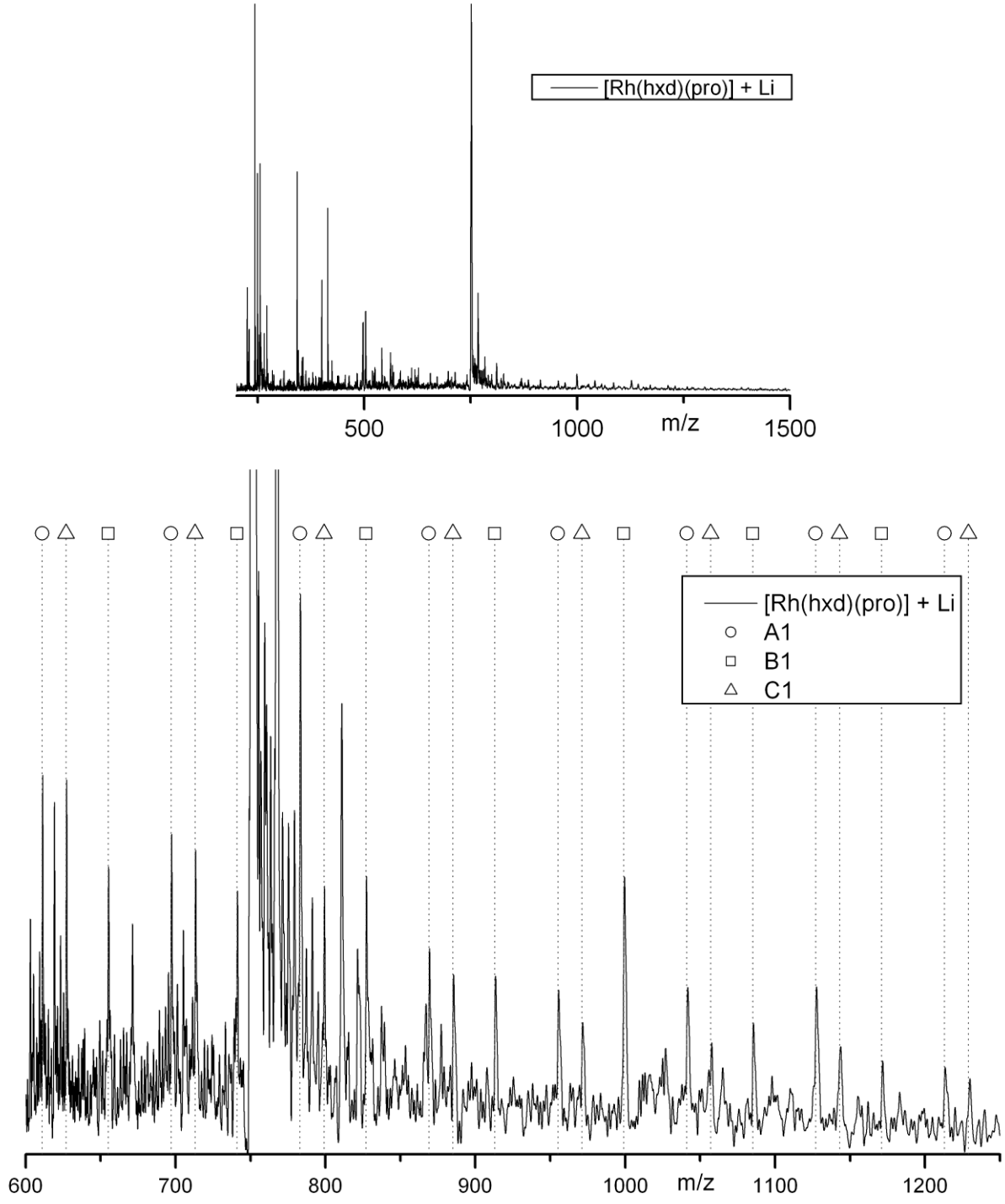

Figure S3-2: MALDI-ToF mass spectra of [Rh(hxd)(L-pro)] (**4**) after addition of CF_3CO_2Li, complete spectrum (above) and selected part with assigned series (below). The peaks between 750 and 790 Da are detected more often after addition of Li.

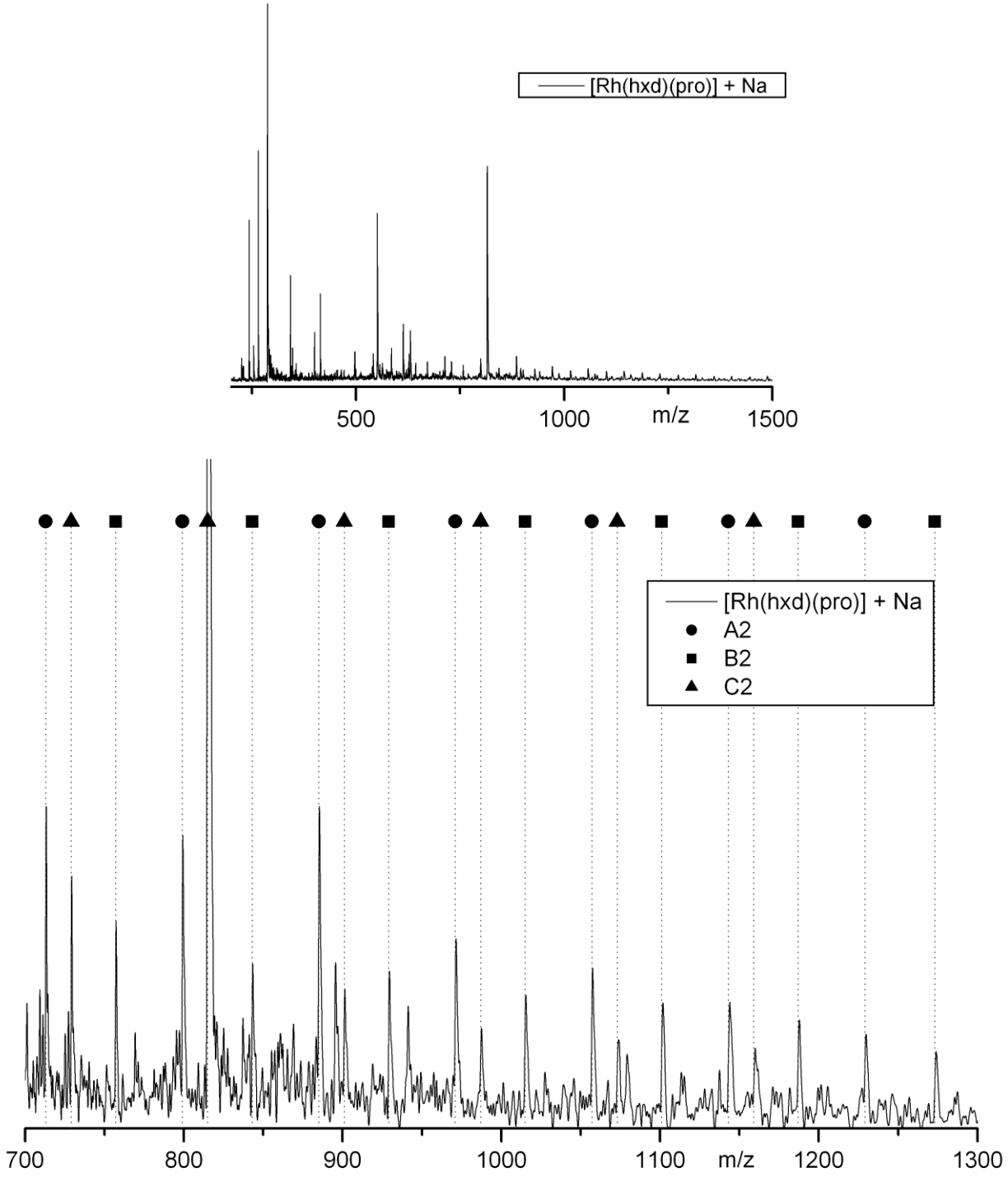

Figure S3-3: MALDI-ToF mass spectra of [Rh(hxd)(L-pro)] (**4**) after addition of CF_3CO_2Na, complete spectrum (above) and selected part with assigned series (below).

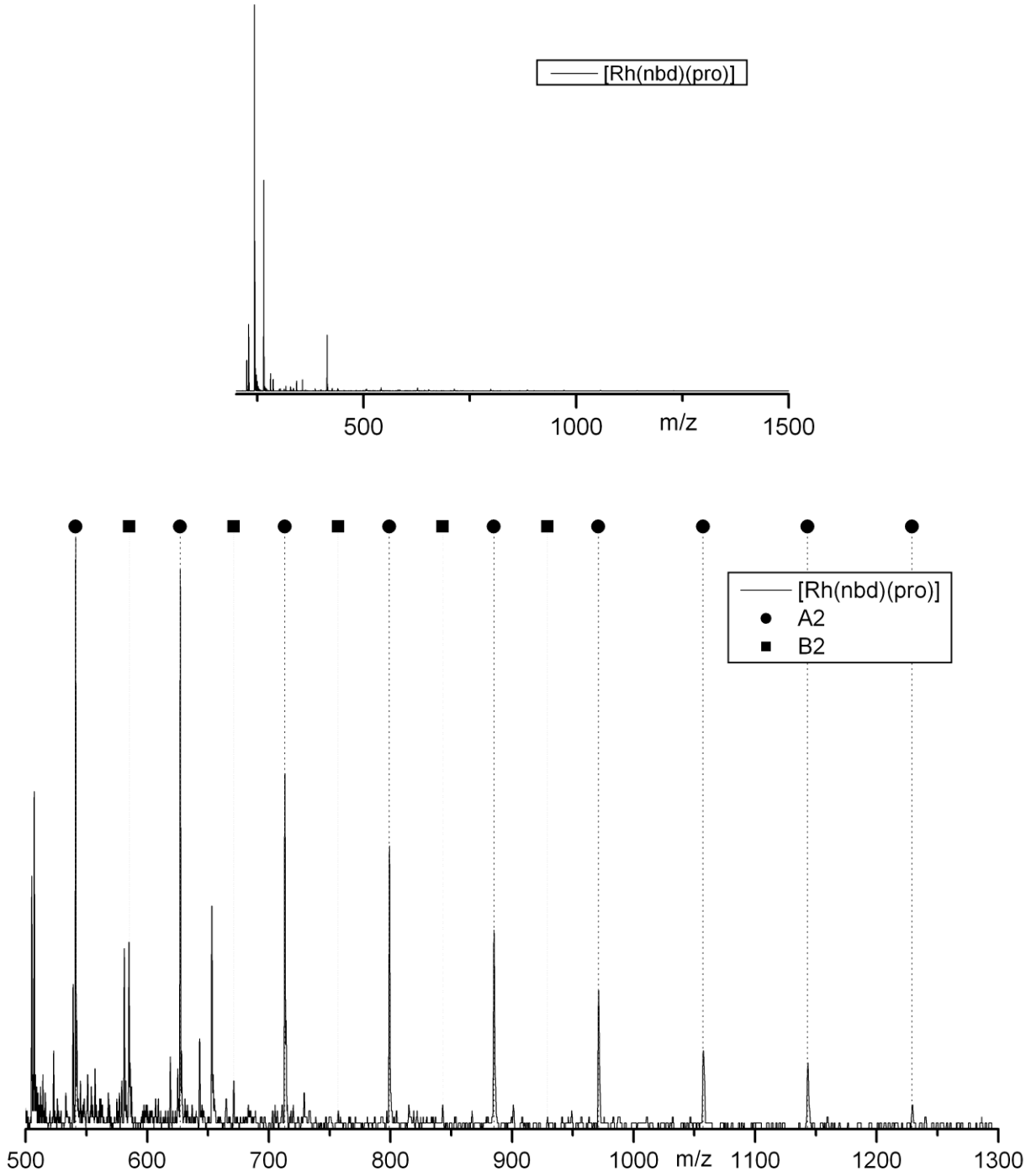

Figure S3-4: MALDI-ToF mass spectra of [Rh(nbd)(L-pro)] (**3**), complete spectrum (above) and selected part with assigned series (below). Although lower in intensity, C2 can be detected as well.

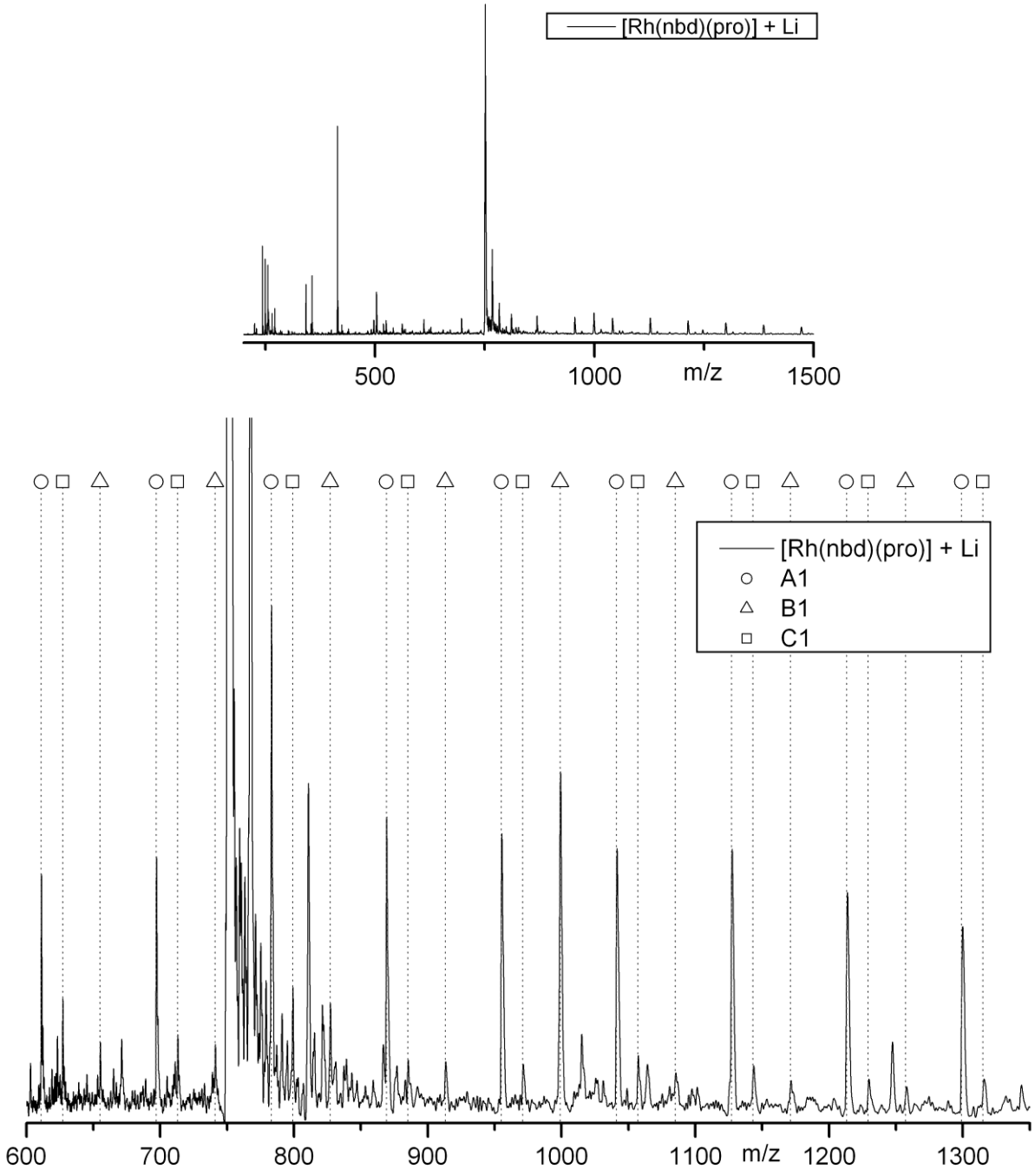

Figure S3-5: MALDI-ToF mass spectra of [Rh(nbd)(L-pro)] (**3**) after addition of CF_3CO_2Li, complete spectrum (above) and selected part with assigned series (below). The peaks between 750 and 790 Da are detected more often after addition of Li.

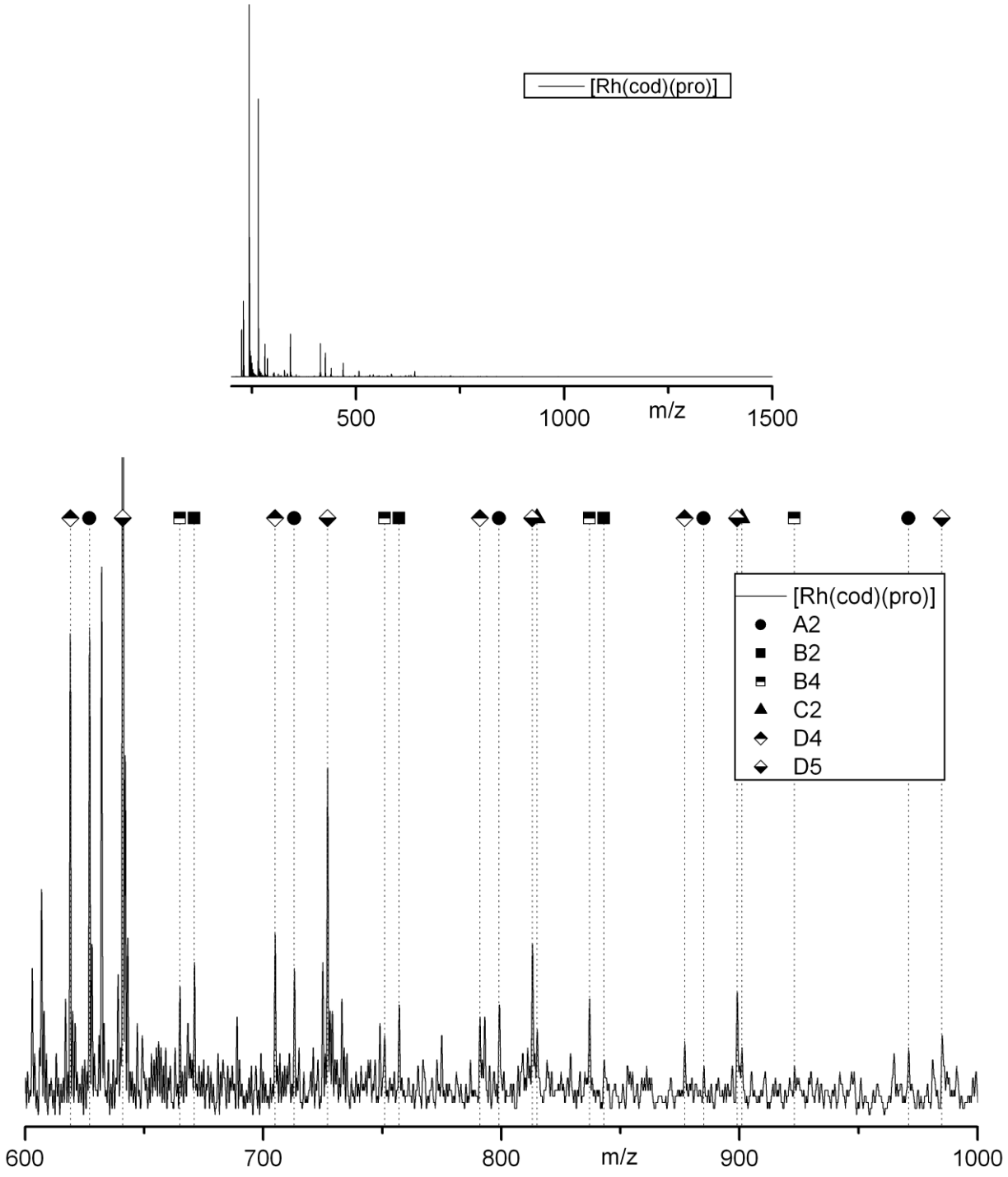

Figure S3-6: MALDI-ToF mass spectra of [Rh(cod)(L-pro)] (**1**), complete spectrum (above) and selected part with assigned series (below).

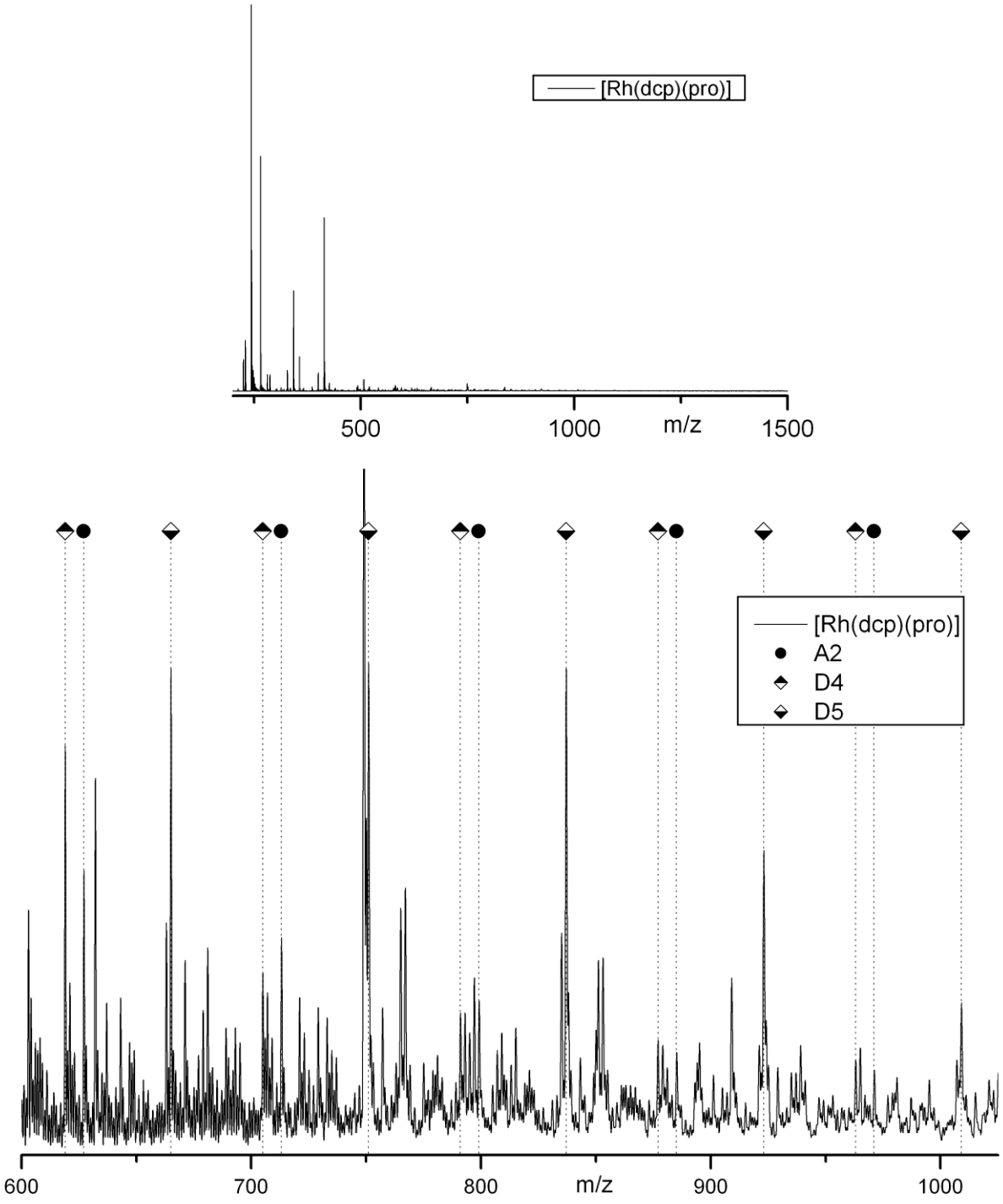

Figure S3-7: MALDI-ToF mass spectra of [Rh(dcp)(L-pro)] (**2**), complete spectrum (above) and selected part with assigned series (below).

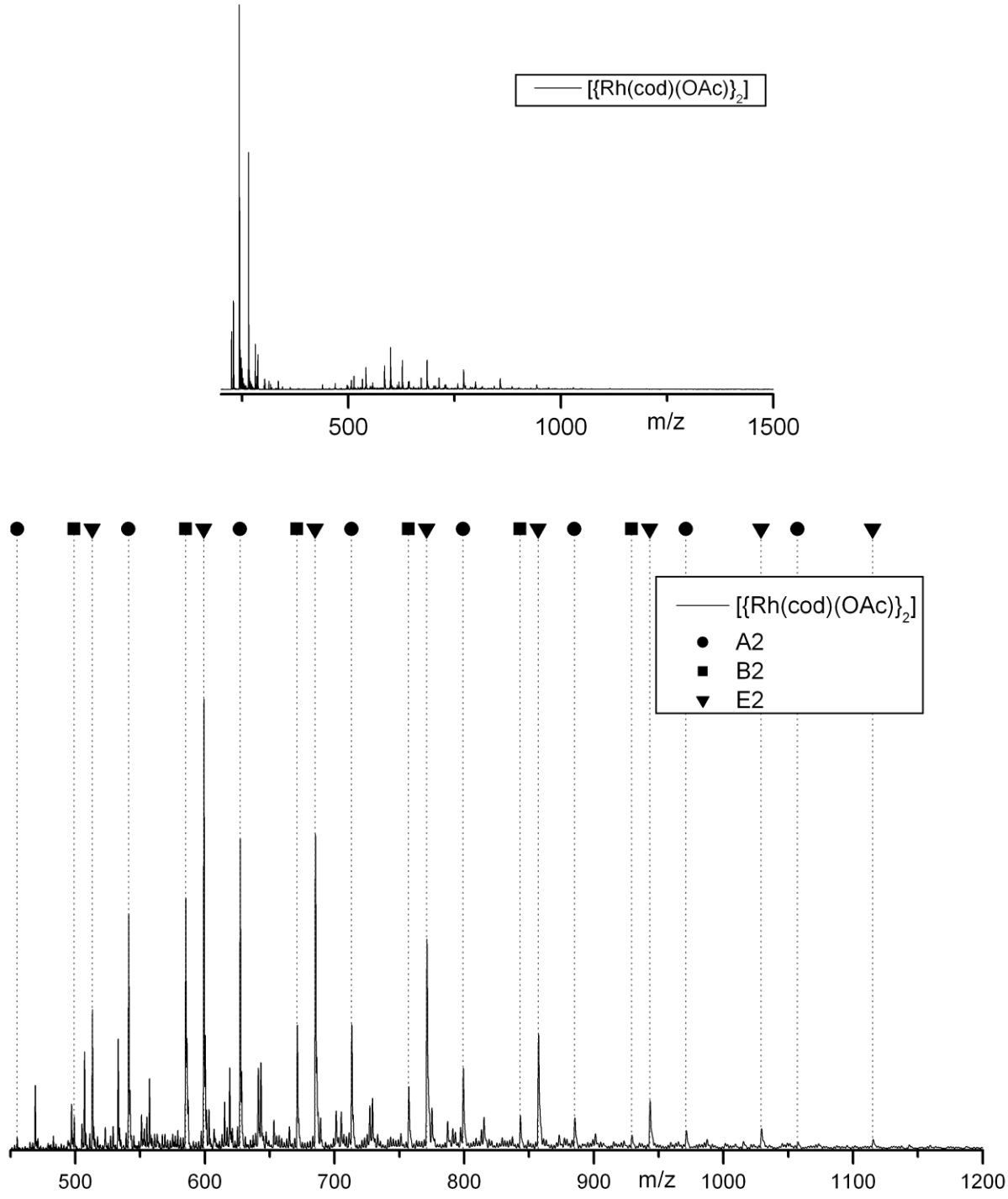

Figure S3-8: MALDI-ToF mass spectra of [{Rh(cod)(OAc)}$_2$] (**6**), complete spectrum (above) and selected part with assigned series (below). Although lower in intensity, other series can be detected as well (*e.g.* D4) but are omitted for clarity.

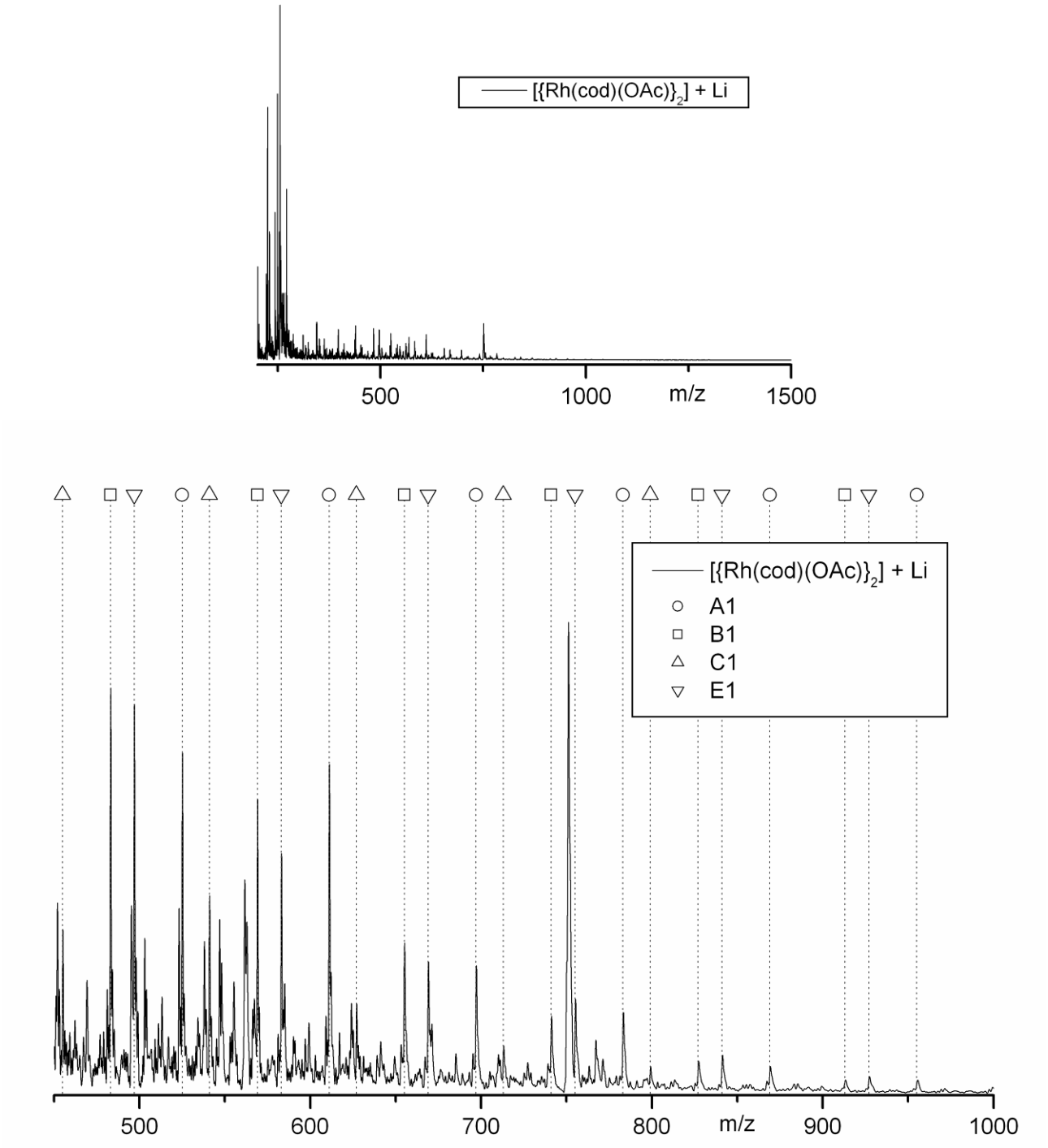

Figure S3-9: MALDI-ToF mass spectra of [{Rh(cod)(OAc)}$_2$] (**6**) after addition of CF_3CO_2Li, complete spectrum (above) and selected part with assigned series (below). The peak at 750 Da is detected more often after addition of Li.

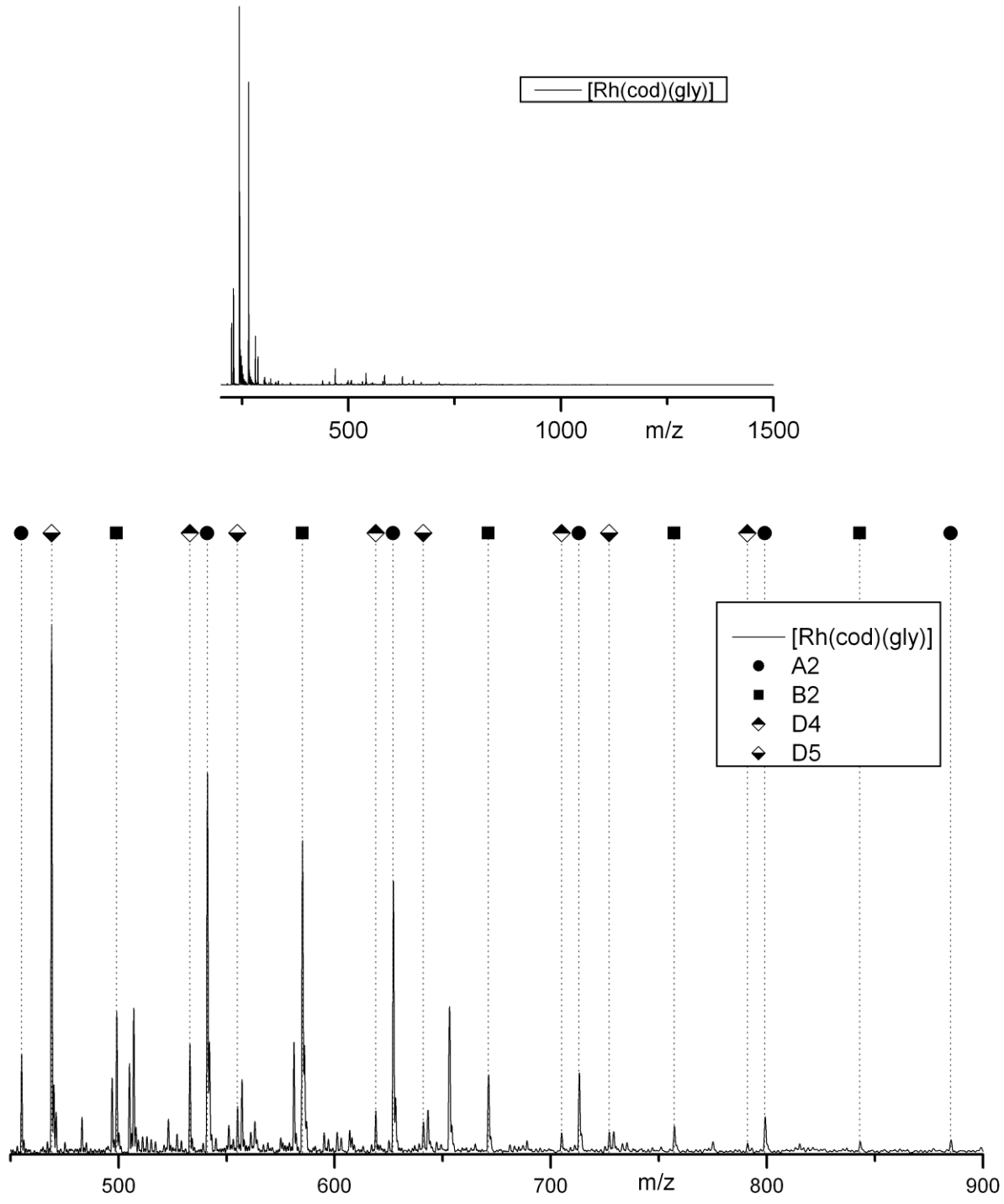

Figure S3-10: MALDI-ToF mass spectra of [Rh(cod(gly)] (**7**), complete spectrum (above) and selected part with assigned series (below).

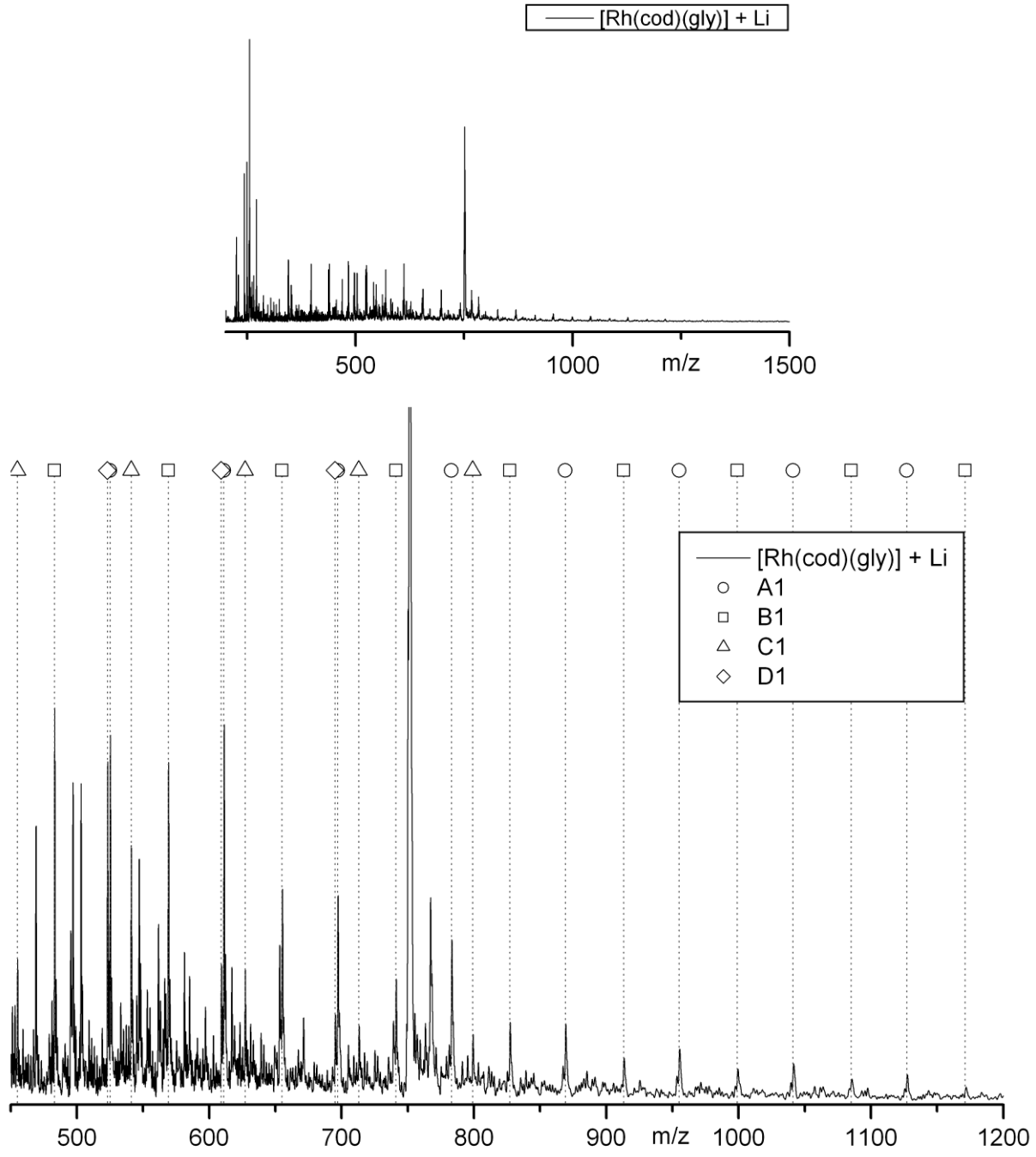

Figure S3-11: MALDI-ToF mass spectra of [Rh(cod)(gly)] (**7**) after addition of CF_3CO_2Li, complete spectrum (above) and selected part with assigned series (below).

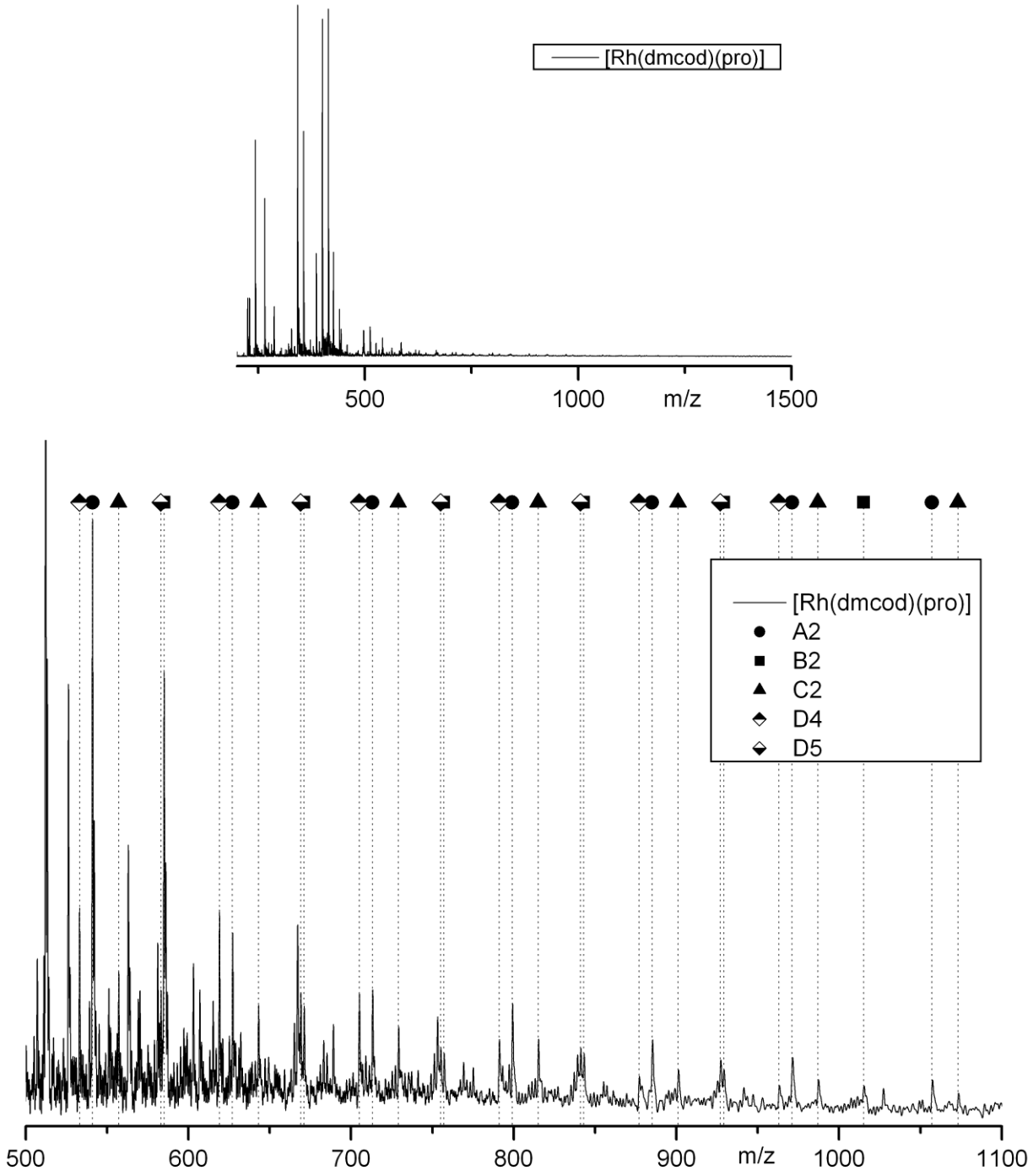

Figure S3-12: MALDI-ToF mass spectra of [Rh(dmcod)(L-pro)] (**5**), complete spectrum (above) and selected part with assigned series (below).

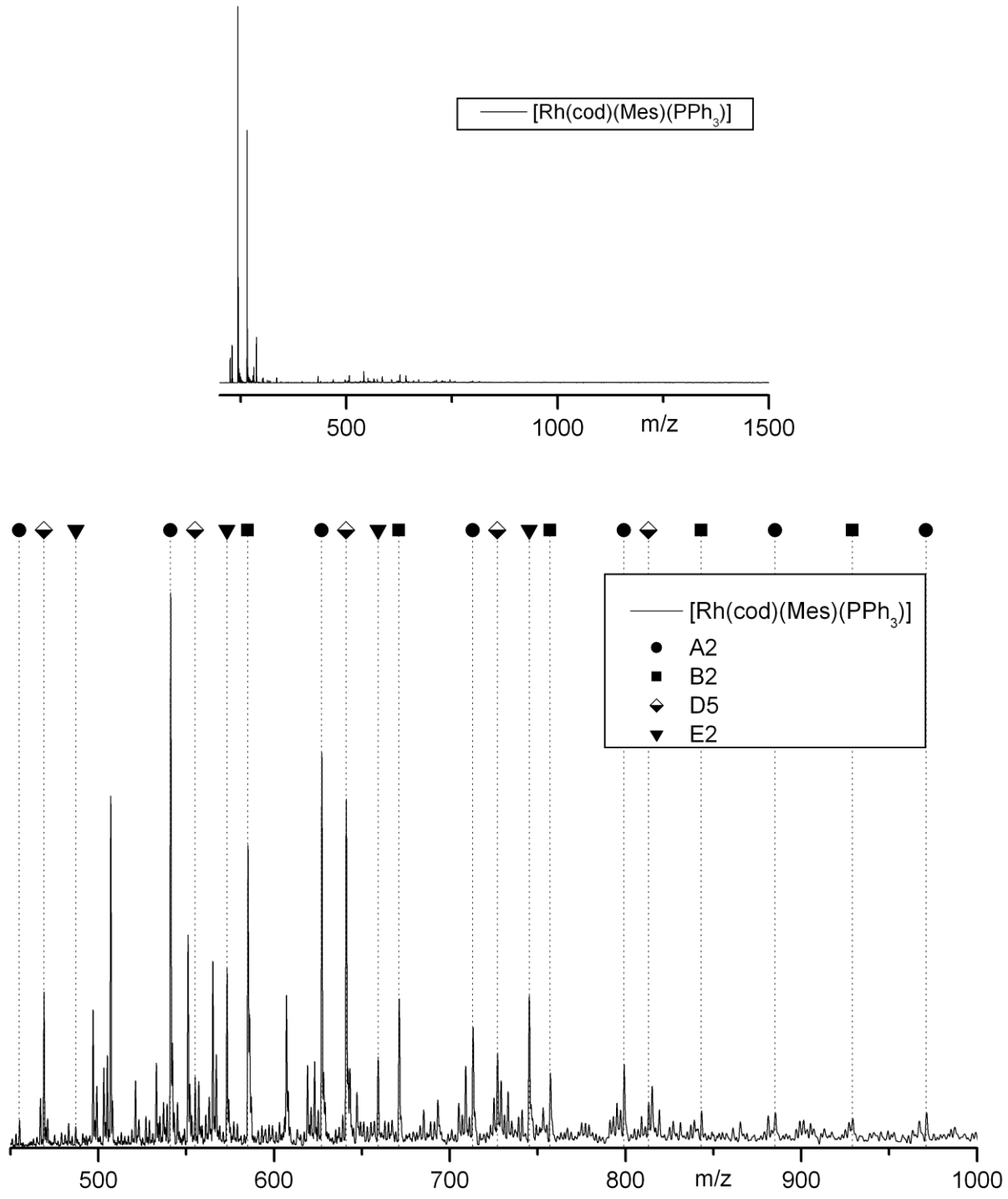

Figure S3-13: MALDI-ToF mass spectra of [Rh(cod)(Mes)(PPh_3)] (**8**), complete spectrum (above) and selected part with assigned series (below).

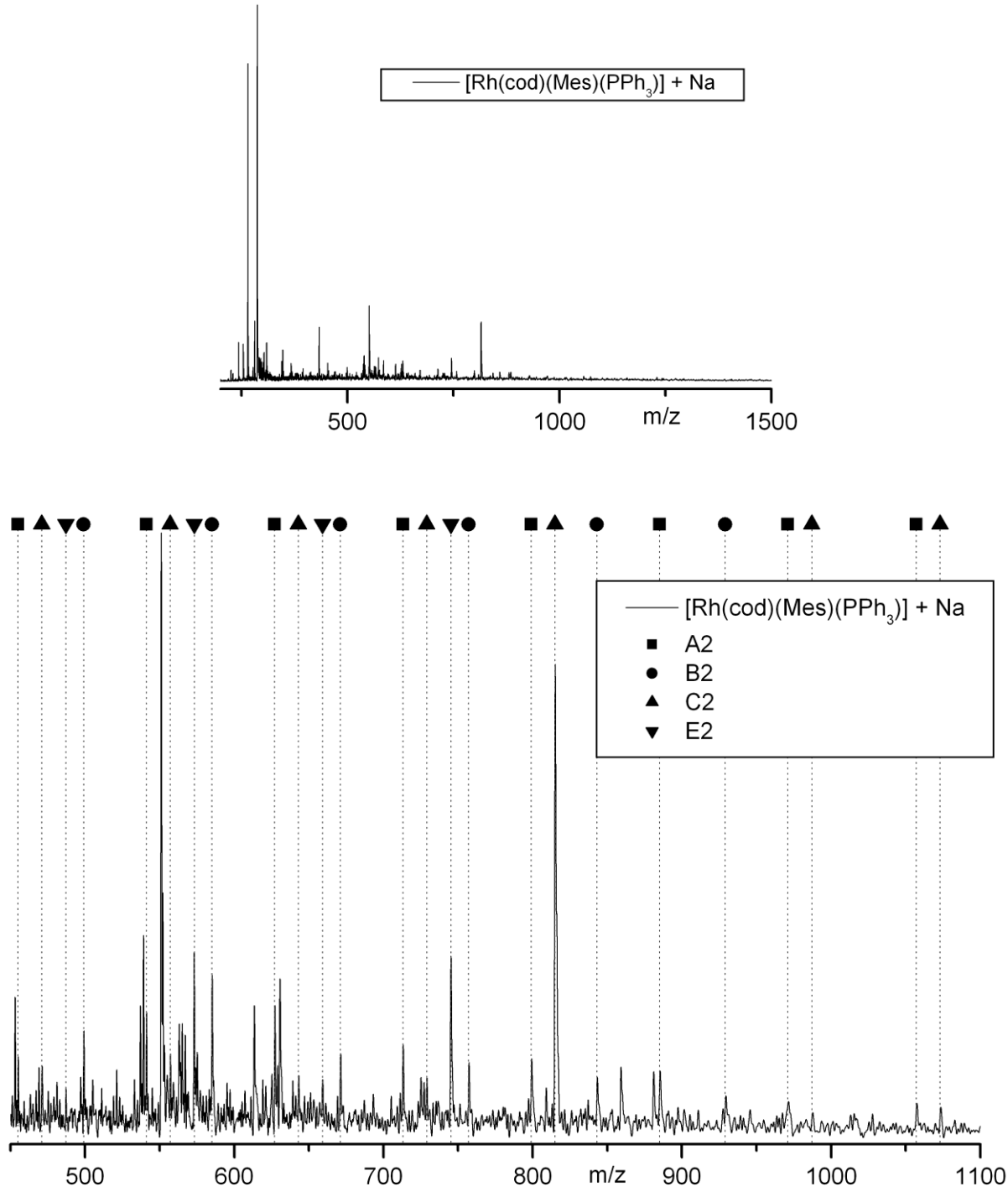

Figure S3-14: MALDI-ToF mass spectra of [Rh(cod)(Mes)(PPh_3)] (**8**) after addition of CF_3CO_2Na, complete spectrum (above) and selected part with assigned series (below).

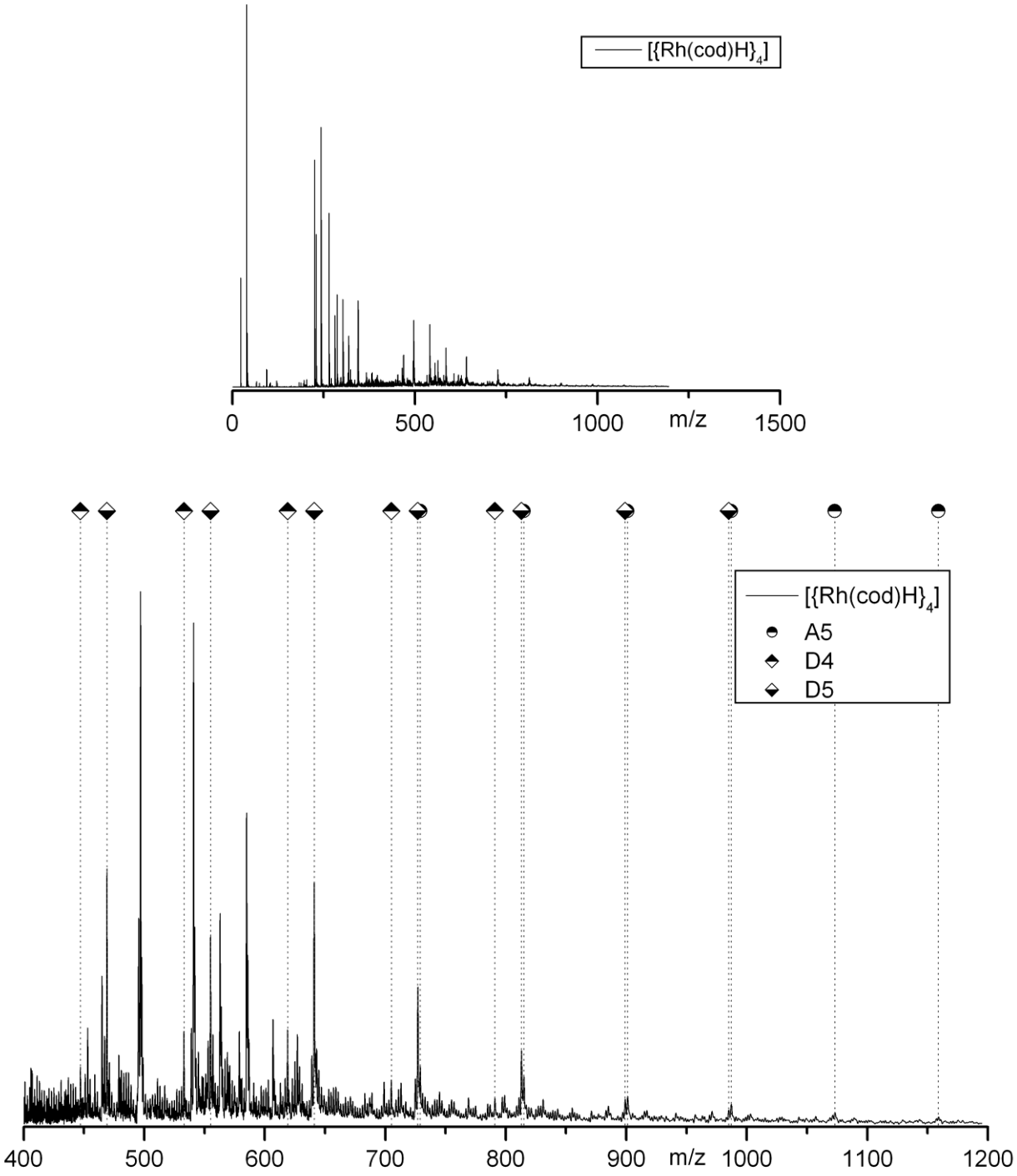

Figure S3-15: MALDI-ToF mass spectra of [{Rh(cod)H}$_2$] (**9**), complete spectrum (above) and selected part with assigned series (below).

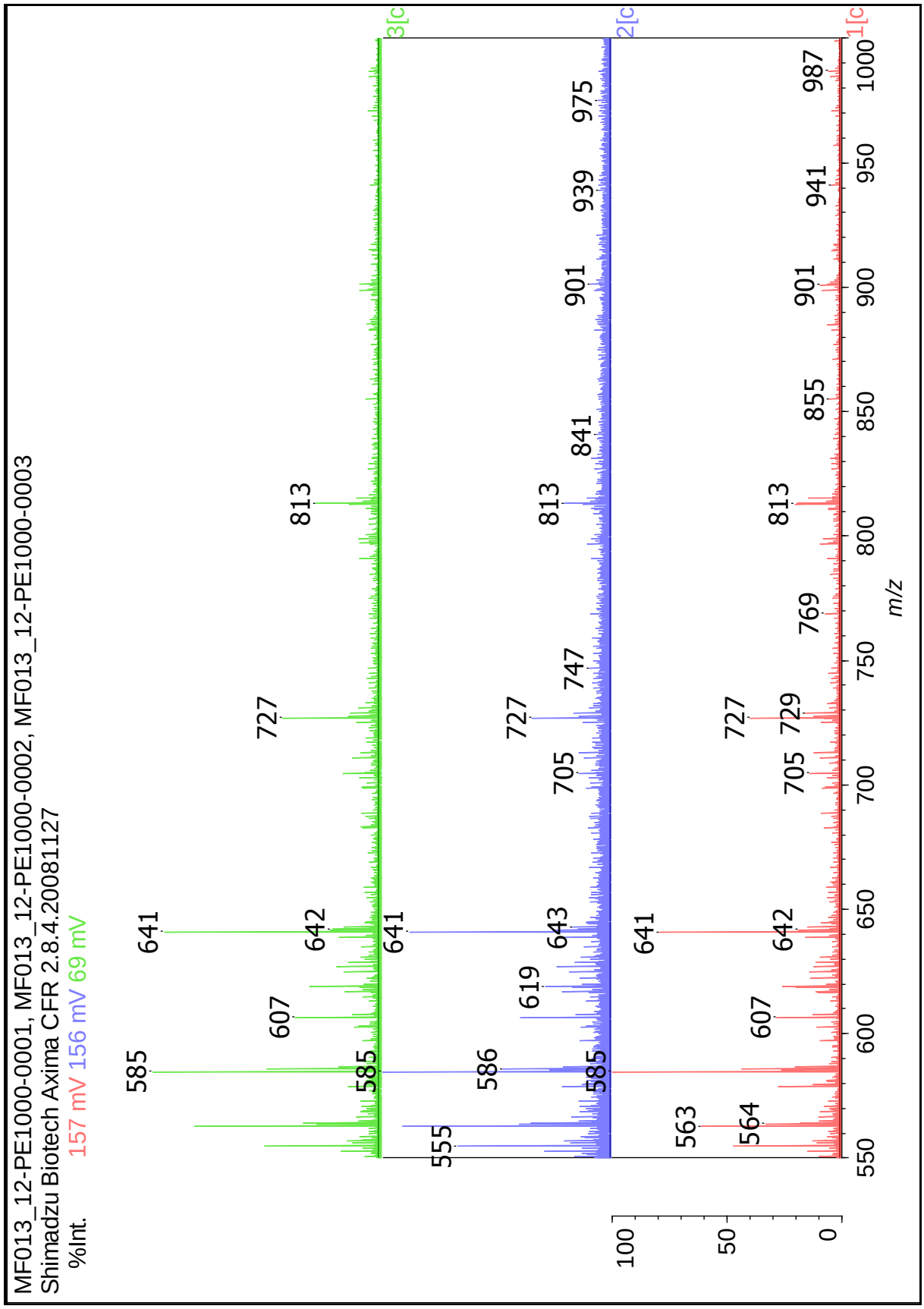

Figure S3-16: MALDI-ToF mass spectra of [{Rh(cod)H}$_2$] (**9**) in three different measurements. In all cases there is a shift to the saturated chains at higher molecular weights.

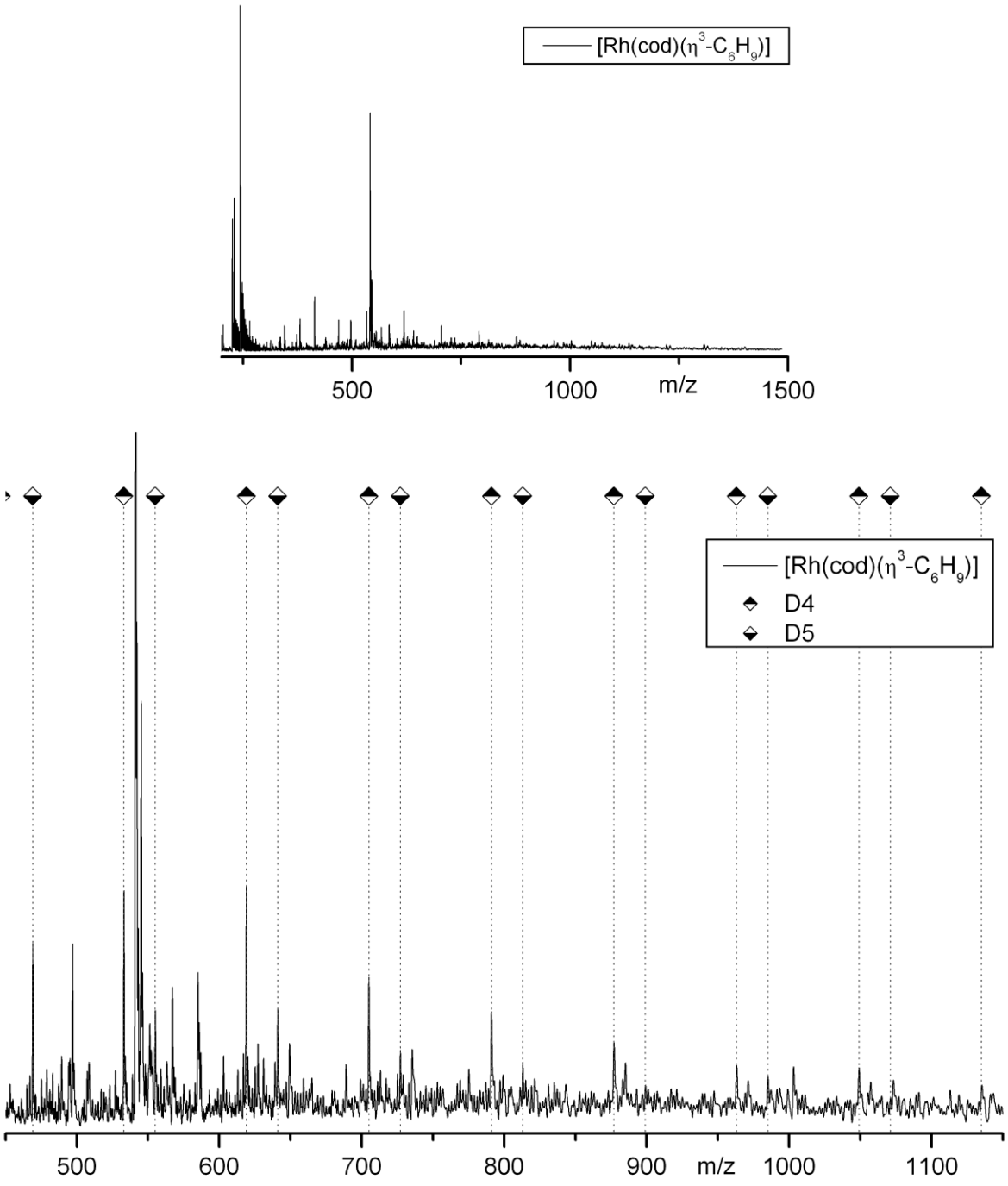

Figure S3-17: MALDI-ToF mass spectra of [Rh(cod)(η^3-C_6H_9)] (**10**), complete spectrum (above) and selected part with assigned series (below).

S4. SEC traces

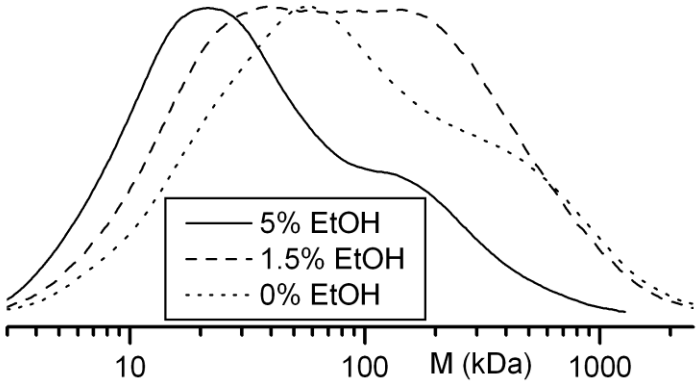

Figure S4-1. SEC-traces of polymer samples obtained in diluted reaction mixtures (70 ml solvent) of precatalyst **1** and EDA in chloroform containing different amounts of EtOH (the peak intensities were adjusted to obtain a clear picture).

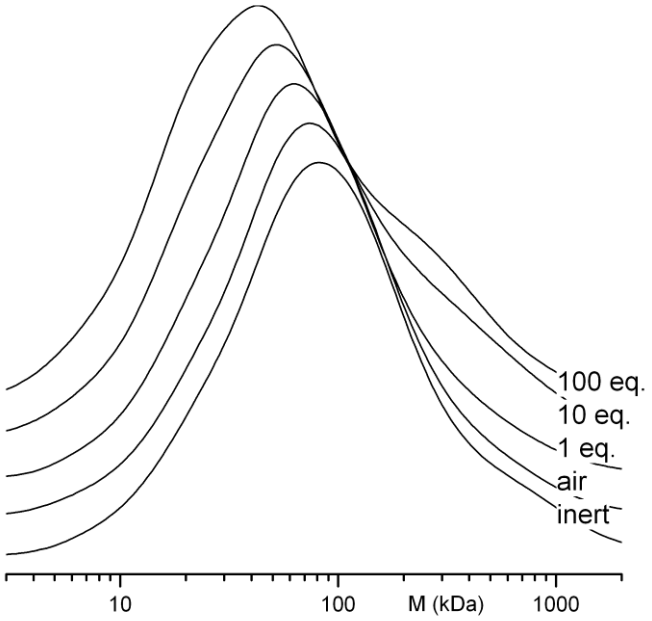

Figure S4-2. SEC-traces of polymer samples obtained in reaction mixtures of precatalyst **1** and EDA in pure chloroform with different amounts of added water (the peak intensities were adjusted to obtain a clear picture).

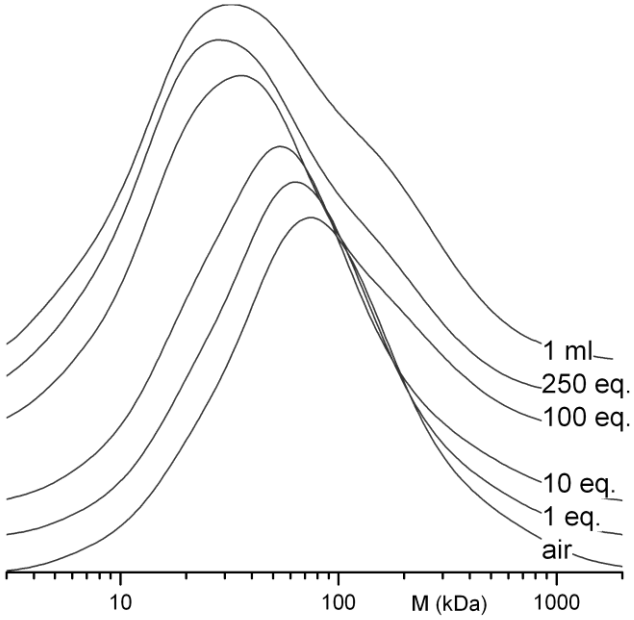

Figure S4-3. SEC-traces of polymer samples obtained in reaction mixtures of precatalyst **1** and EDA in pure chloroform with different amounts of added methanol (the peak intensities were adjusted to obtain a clear picture).

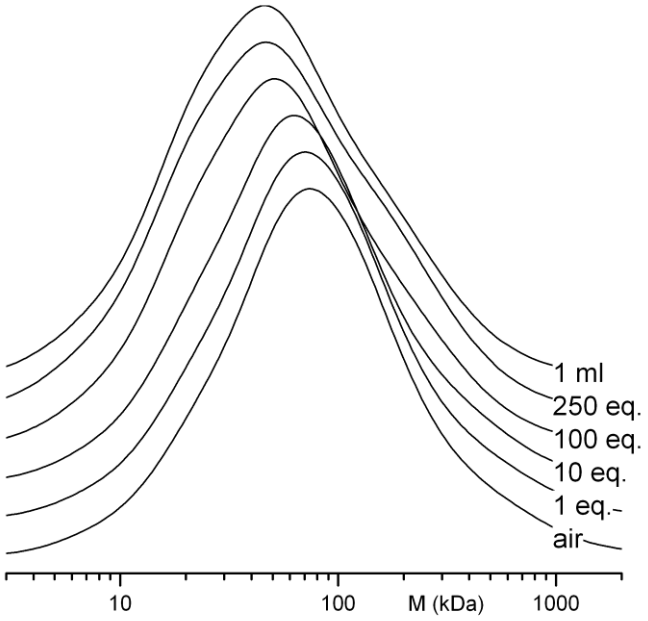

Figure S4-4. SEC-traces of polymer samples obtained in reaction mixtures of precatalyst **1** and EDA in pure chloroform with different amounts of added ethanol (the peak intensities were adjusted to obtain a clear picture).

S5. Characterization of the MeOH soluble material obtained in the presence of alcohols

Carbene polymerization often leads to formation of some ill-defined atactic oligomers as the side-product. We usually separate these oligomers from the polymer fraction by precipitation of the syndiotactic polymer with methanol (as described in our earlier studies). The methanol soluble oligomeric fraction is then obtained by evaporation of the solvent.

However, the polymerization reaction in the presence of alcohols leads to markedly shorter syndiotactic polymers, which are in part soluble in MeOH. The above procedure therefore leads to a methanol soluble "oligomeric" fraction, which is in fact a mixture of the undesired ill-defined atactic oligomeric byproducts and a shorter fraction of the well-defined syndiotactic polymer. The polymer fraction in this mixture is substantially longer than the atactic oligomers, but short enough to be MeOH soluble.

For the reaction performed in the presence of 1 ml of MeOH, we decided to analyze the thus obtained "oligomeric" material better. We therefore separated three oligomeric fractions over a silica column using subsequently DCM, *i*-propanol and ethyl acetate as the eluent. The obtained fractions were dried in vacuo to evaporate the solvent and any possible volatile side-products. After drying, the samples were analyzed by SEC, ^{1}H NMR and ^{13}C APT NMR spectroscopy.

Fraction 1 proves to be a shorter fraction of the syndiotacic polymer (short enough to be soluble in MeOH). Fraction 2 and 3 seem to contain (some) syndiotactic material, but are much less defined than fraction 1, with indications for branches and (partly) atactic material in the NMR spectra.

The SEC traces of the three oligomeric fractions are shown in Figure S5-1. For comparison a SEC trace of the obtained methanol insoluble polymeric fraction is included. The oligomeric fraction 1 has a relatively narrow molecular weight distribution around 3700 Da, which is only slightly shorter than the main methanol-insoluble polymeric fraction obtained under these conditions. The second (bimodal distribution) and the third fraction have broader molecular weight distributions, and these oligomers are much shorter.

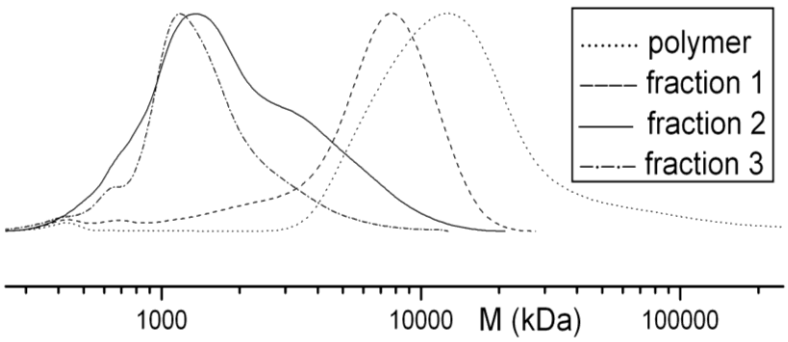

Figure S5-1. SEC results of the polymeric and the oligomeric fractions formed in the presence of 1 ml of MeOH.

The ^{1}H NMR spectra of the three oligomer fractions are shown in Figure S5-2. All the fractions show peaks at δ 4.1 ppm and δ 1.2 ppm (CH_2 and the CH_3 of the ester). The peak of the CH backbone at δ 3.2 ppm is much broader in fraction 2 and 3 (indicating a lower tacticity) and looks slightly different in fraction 2 and 3. The first fraction shows the sharpest peaks, which are comparable with the ^{1}H NMR spectrum of the methanol-insoluble syndiotactic polymeric fraction.

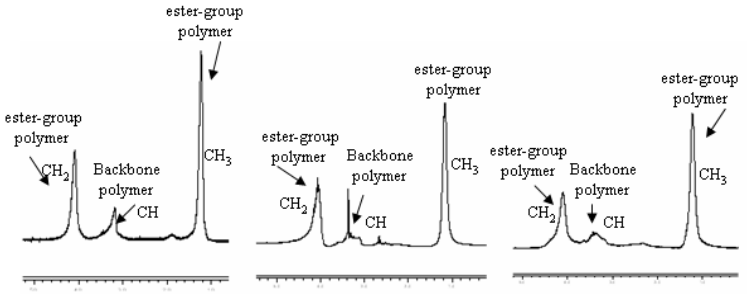

Figure S5-2: ^{1}H NMR spectra of the three fractions (left = fraction 1, middle = fraction 2, right = fraction 3) (400 MHz, RT, $CDCl_3$).

The ^{13}C APT NMR spectra of the three oligomer fractions are shown in Figure S5-3. Fraction 1 again shows only the expected shifts of the syndiotactic polymer (Figure S5-4), but the spectra of the second and third fraction reveal extra peaks at δ 62 ppm and between δ 40 ppm and δ 20 ppm. These signals indicate the presence of secondary and quaternary carbon atoms, and point to the formation of branched (partly atactic) oligomeric products. Signals for the expected -CH_2COOEt end-groups formed by alcohol-mediated chain transfer, broadened by the molecular weight distribution of these short oligomers, are visible for fractions 2 and 3.

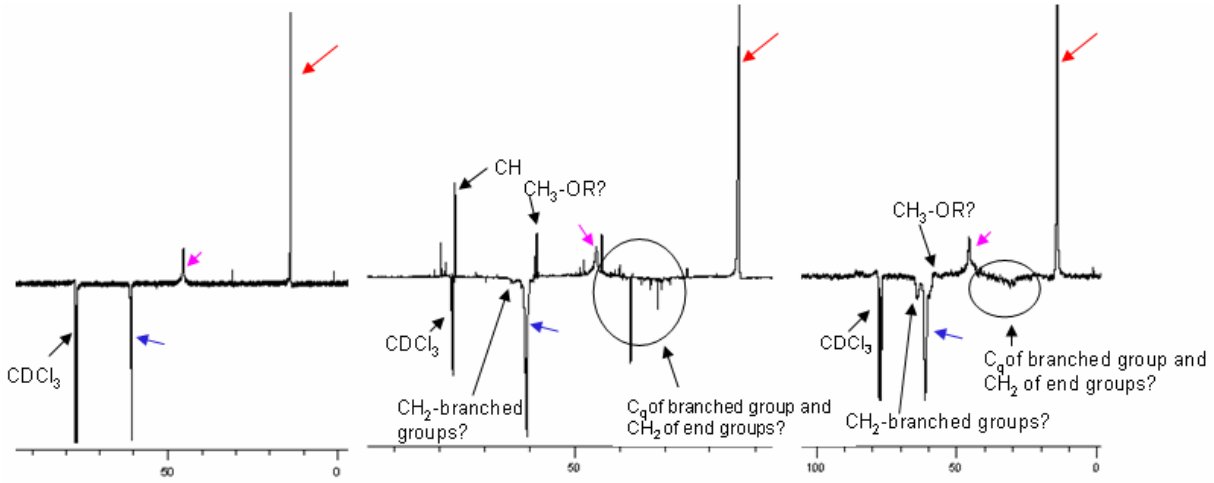

Figure S5-3. ^{13}C APT NMR spectra of the three oligomer fractions with chemical shifts in ppm (left = fraction 1, middle = fraction 2, right = fraction 3).

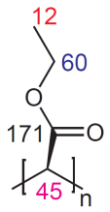

Figure S5-4. ^{13}C NMR chemical shifts of the polymer in ppm.